

Unsupervised Domain Adaptive Lane Detection via Contextual Contrast and Aggregation

Kunyang Zhou, Yunjian Feng, and Jun Li, *Senior Member, IEEE*

Abstract—This paper focuses on two crucial issues in domain-adaptive lane detection, i.e., how to effectively learn discriminative features and transfer knowledge across domains. Existing lane detection methods usually exploit a pixel-wise cross-entropy loss to train detection models. However, the loss ignores the difference in feature representation among lanes, which leads to inefficient feature learning. On the other hand, cross-domain context dependency crucial for transferring knowledge across domains remains unexplored in existing lane detection methods. This paper proposes a method of Domain-Adaptive lane detection via Contextual Contrast and Aggregation (DACCA), consisting of two key components, i.e., cross-domain contrastive loss and domain-level feature aggregation, to realize domain-adaptive lane detection. The former can effectively differentiate feature representations among categories by taking domain-level features as positive samples. The latter fuses the domain-level and pixel-level features to strengthen cross-domain context dependency. Extensive experiments show that DACCA significantly improves the detection model’s performance and outperforms existing unsupervised domain adaptive lane detection methods on six datasets, especially achieving the best performance when transferring from CULane to Tusimple (92.10% accuracy), Tusimple to CULane (41.9% F1 score), OpenLane to CULane (43.0% F1 score), and CULane to OpenLane (27.6% F1 score).

Index Terms—Unsupervised domain adaptation, Lane detection, Contextual contrast, Contextual aggregation.

I. INTRODUCTION

Lane detection is crucial in autonomous driving and advanced driver assistance systems. Benefitting from developing convolutional neural networks, deep learning-based lane detection methods [1], [2] demonstrate greater robustness and higher accuracy than traditional methods [3]. To train a robust lane detection model, a high-quality dataset is necessary. However, acquiring high-quality labeled data is laborious and costly. Simulation is a low-cost way to obtain training pictures. Nevertheless, the detection performance may be degraded after transitioning from the virtual (source domain) to the real (target domain). Unsupervised domain adaptation (UDA) has been proposed to solve this problem [4], [5].

Recently, UDA has been successfully applied in the image segmentation task [5], [6], significantly improving the segmentation performance. However, applying existing unsupervised domain-adaptive segmentation methods to lane detection

does not yield satisfactory results, even inferior to those of supervised training, as revealed in [7]. We consider the cross-entropy loss adopted in these methods only focuses on pulling similar features closer but ignores different features across categories, making these methods inefficient in learning discriminative features of different categories [8]. Contrastive learning [9], [10] is expected to solve this problem by appropriately selecting positive and negative samples. However, segmentation models may generate false pseudo-labels on the input image for the unlabeled target domain, causing false assignments of positive samples. On the other hand, cross-domain context dependency is essential for adaptive learning of cross-domain context information [11], which is overlooked by many existing domain adaptive lane detection methods, e.g. [12] and [13]. In MLDA [7], an Adaptive Inter-domain Embedding Module (AIEM) is proposed to aggregate contextual information, but it is limited to performing on a single image and disregards useful contextual information from other images. How to effectively leverage the potential of cross-domain context dependency in domain-adaptive lane detection remains a challenging topic.

This paper presents a novel Domain-Adaptive lane detection via Contextual Contrast and Aggregation (DACCA) to address the aforementioned issues. As shown in Fig. 1, two positive sample memory modules (PSMMs) are adopted to save domain-level features for each lane in both source and target domains. We select two corresponding domain-level features as positive samples from both source and target PSMMs for each lane pixel in an input image. Subsequently, the selected domain-level features are aggregated with the original pixel feature to enrich the cross-domain contextual information. In addition, we pair the aggregated features with the source and target positive samples to avoid the false assignment of positive samples in the cross-domain contrastive loss.

The main contributions of this paper are as follows. **(1)** We propose a novel cross-domain contrastive loss to learn discriminative features and a novel sampling strategy to fully utilize the potential of contrastive loss without modifying an existing contrastive loss. **(2)** A novel domain-level feature aggregation module combining pixel-level and domain-level features is presented to enhance cross-domain context dependency, Aggregating domain-level features, instead of feature aggregation of mini-batches or individual images, is a fresh perspective. **(3)** Extensive experiments show that our method can significantly improve the baseline performance on six public datasets. Remarkably, compared with existing domain adaptive lane detection methods, our approach achieves the best results when transferring from CULane to Tusimple, Tusimple to CULane,

This work was supported in part by the National Key Research and Development Program of China under Grant 2021YFF0500904, and Shenzhen Fundamental Research Program under Grant JCYJ20190813152401690, and Qingdao New Qianwan Container Terminal (QQCTN). (Corresponding author: Jun Li.)

K. Zhou, Y. Feng, and J. Li are with the Ministry of Education Key Laboratory of Measurement and Control of CSE, Southeast University, Nanjing 210096, China (e-mail: kunyangzhou@seu.edu.cn; fengyunjian@seu.edu.cn; j.li@seu.edu.cn).

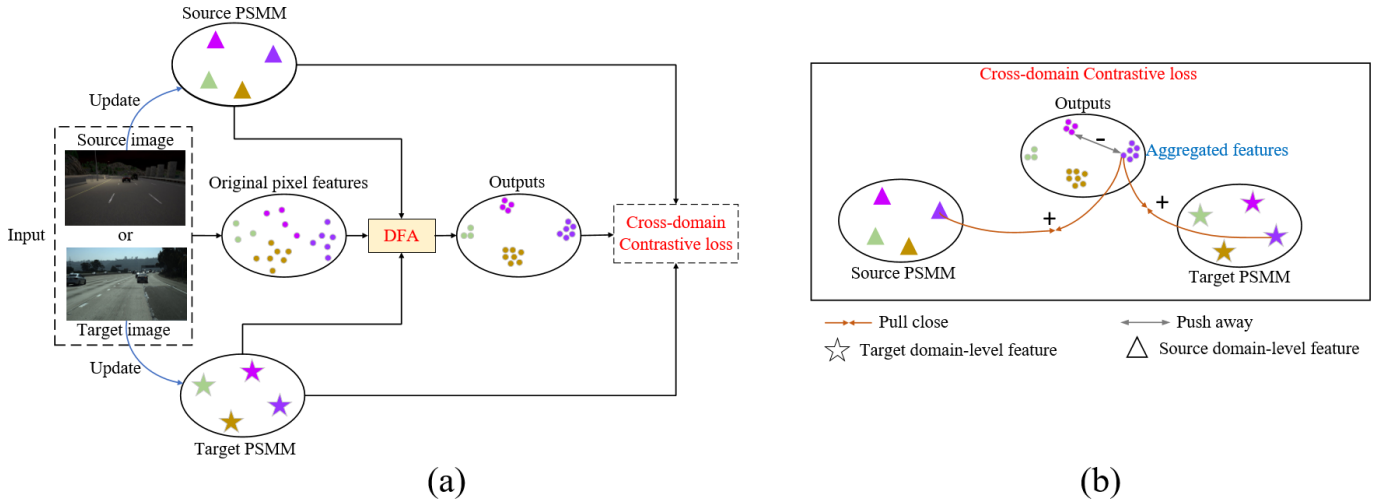


Fig. 1: Diagrams of our DACCA. (a) The main flowchart, and (b) the proposed cross-domain contrastive loss, where DFA is the abbreviation of domain-level feature aggregation. Different colors in the original pixel features represent different lane features.

OpenLane to CULane, and CULane to OpenLane.

The rest of the paper is organized as follows. Section II reviews the related work and Section III details DACCA. Extensive experiments are conducted in Section IV. Section V concludes this paper.

II. RELATED WORK

A. Lane Detection

Traditional lane detection mainly depends on image processing operators, e.g., Hough transforms [3]. Although they can quickly achieve high detection accuracy in specific scenarios, their generalization ability is too poor to apply to complex scenarios. Deep learning-based lane detection has received increasing attention, including segmentation-based methods [1], [14], anchor-based methods [15], [16], and parameter-based methods [17], [18]. SCNN [1] is one of the typical segmentation-based methods using a message-passing module to enhance visual evidence. Unlike pixel-wise prediction in segmentation-based methods, anchor-based methods regress accurate lanes by refining predefined lane anchors. For example, using a lightweight backbone, UFLD [19] pioneers row anchors in real-time lane detection. Parameter-based methods treat lane detection as the parameter modeling problem and regress the parameters of the lane. PolyLaneNet [17] models a lane as a polynomial function and regresses the parameters of the polynomial. Although parameter-based methods have a faster inference speed than the other two methods, they struggle to achieve a higher performance. In this paper, we consider segmentation-based domain-adaptive lane detection.

B. Unsupervised Domain Adaptation

Domain adaptation has been widely studied to address the domain discrepancy in feature distribution, usually, implemented through adversarial training and self-training. Adversarial training [20] eliminates the differences in feature

distribution between the source and target domains by adversarial approaches. Different from adversarial training, self-training [21], [6] trains a model in the target domain using generated pseudo labels. On the other hand, the contrastive loss is introduced as an auxiliary loss to improve the model's robustness. CDCL [22] takes labels and pseudo-labels as positive samples in the source and target domain, respectively. However, the model may generate false pseudo labels in the unlabeled target domain, leading to false positive sample assignments. There exists some works [23], [24], [25], [26], [27] taking positive samples from the prototypes to achieve accurate positive sample assignments. CONFETI [23] adopts the pixel-to-prototype contrast to enhance the feature-level alignment. CONFETI only uses a prototype to save source and target domain features, but we think this way is inappropriate because the feature distribution between the two domains is different. In our work, we use two PSMMs to save features of two domains separately and take the domain-level features as positive samples. In addition, we also optimize the sample selection policy in the contrastive loss but most works ignore it.

C. Unsupervised Domain Adaptive Lane Detection

Due to the lack of a domain adaptive lane detection dataset, early studies [12], [28] focus on synthetic-to-real or simulation-to-real domain adaptation. Their generalizability in real-world scenarios is not satisfactory with low-quality synthetic and simulation images. [13] establishes a specific dataset for domain adaptive lane detection and directly apply a general domain adaption segmentation method to this dataset. However, it does not yield good results, since conventional domain adaptive segmentation methods generally assume the presence of salient foreground objects in the image, occupying a significant proportion of the pixels. On the other hand, lane lines, which occupy a relatively small proportion of the image, do not exhibit such characteristics. To solve this problem,

MLDA [7] introduces an AIEM to enhance the feature representation of lane pixel by aggregating contextual information in a single image. Unfortunately, in this way, useful contextual information from other images may be ignored. Instead, we propose to aggregate the domain-level features with pixel-level features.

D. Context Aggregation

Performing contextual information aggregation for pixel-level features can effectively improve segmentation performance in semantic segmentation. In supervised methods, common context information aggregation modules, e.g., ASPP [29], PSPNet [30], OCRNet [31], and MCIBI [32], only aggregate features within a single domain instead of both target and source domains. In UDA, some methods try to design modules to aggregate contextual features by attention mechanisms, such as cross-domain self-attention [33], and context-aware mixup [34]. However, all existing cross-domain feature aggregation methods only fuse a mini-batch of contextual features. In contrast to previous works, our method tries to simultaneously fuse features from the whole target and source domains to enhance the cross-domain context dependency.

III. METHOD

As illustrated in Fig. 2, the network is self-trained in our DACCA, where the student model is trained in both the labeled source domain and the unlabeled target domain with pseudo-labels generated by the teacher model. DACCA has two key components, i.e., cross-domain contrastive loss and domain-level feature aggregation.

A. Self-Training

In UDA, a segmentation-based lane detection model s_θ is trained using source images $X^s = \{x_S^k\}_{k=1}^{N_s}$ with labels $Y^s = \{y_S^k\}_{k=1}^{N_s}$, to achieve a good performance on the unlabeled target images $X^t = \{x_T^k\}_{k=1}^{N_t}$, where N_s and N_t are the number of source and target images, respectively. y_S^k is a one-hot label. Pixel-wise cross-entropy loss L_S^k is adopted to train s_θ in the source domain.

$$L_S^k = - \sum_{i=1}^H \sum_{j=1}^W \sum_{c=1}^{C+1} (y_S^k)_{(i,j,c)} \times \log(s_\theta(x_S^k)_{(i,j,c)}), \quad (1)$$

where C is the number of lanes and class $C + 1$ denotes the background category. H and W are the height and width of x_S^k . However, when transferred to the target domain, s_θ trained in the source domain suffers from performance degradation due to the domain shift. In this paper, we adopt a self-training method [6] to address this issue.

As shown in Fig. 2 (a), in the self-training process, we train two models, i.e., student model s_θ and teacher model t_θ to better transfer the knowledge from the source domain to the target domain. Specifically, t_θ generates the one-hot pseudo-label y_T^k on the unlabeled target image x_T^k .

$$(y_T^k)_{(i,j,c)} = \left[c = \operatorname{argmax}_{c' \in c^*} (t_\theta(x_T^k)_{(i,j,c')}) \right], i \in [0, H], j \in [0, W], \quad (2)$$

where $[\cdot]$ denotes the Iverson bracket and c^* represents the set of all categories. To ensure the quality of pseudo-labels, we filter low-quality pseudo-labels by setting the confidence threshold α_c , i.e.,

$$(y_T^k)_{(i,j,c)} = \begin{cases} (y_T^k)_{(i,j,c)}, & \text{if } (t_\theta(x_T^k)_{(i,j,c)}) \geq \alpha_c \\ 0, & \text{otherwise} \end{cases}. \quad (3)$$

s_θ is trained on both labeled source images and unlabeled target images with pseudo-labels. The same pixel-wise cross-entropy loss L_T^k is used as the loss function in the target domain.

$$L_T^k = - \sum_{i=1}^H \sum_{j=1}^W \sum_{c=1}^{C+1} (y_T^k)_{(i,j,c)} \times \log(s_\theta(x_T^k)_{(i,j,c)}). \quad (4)$$

During training, no gradients are backpropagated into t_θ and the weight of t_θ is updated by s_θ through Exponentially Moving Average (EMA) at every iteration m , denoted by,

$$t_\theta^{m+1} = \beta \times t_\theta^m + (1 - \beta) \times s_\theta^m, \quad (5)$$

where the scale factor β is set to 0.9 empirically. After the training, we use the student model s_θ for inference and produce the final lane detection results.

B. Cross-domain Contrastive Loss

Since the cross-entropy loss is ineffective in learning discriminative features of different lanes, we introduce the category-wise contrastive loss [24] to solve this problem. The formulation of category-wise contrastive loss L_{CL} is written as,

$$L_{CL} = - \frac{1}{C \times M} \sum_{c=1}^C \sum_{p=1}^M \log \left[\frac{e^{\langle V_{cp}, V_c^+ \rangle / \tau}}{e^{\langle V_{cp}, V_c^+ \rangle / \tau} + \sum_{q=1}^N e^{\langle V_{cp}, V_{cpq}^- \rangle / \tau}} \right], \quad (6)$$

where M and N represent the numbers of anchors and negative samples, respectively. V_{cp} is the feature representation of the p -th anchors of class c , used as a candidate for comparison. V_c^+ is the feature representation of the positive sample of class c . V_{cpq}^- denotes the feature representation of the q -th negative samples of the p -th anchors of class c . τ is the temperature hyper-parameter and $\langle \cdot, \cdot \rangle$ is the cosine similarity between features from two different samples.

In the target domain, existing methods either focus on improving the form of contrastive loss [22], introducing extra hyper-parameters, or only select V_c^+ from the current input images [24]. However, the false pseudo-labels generated by t_θ cause the incorrect positive samples assignment, making the contrastive loss ineffective in learning discriminate features of different categories. We develop a sample selection policy without modifying the existing contrastive loss to overcome the difficulty.

Anchor Selection. We choose anchors for each lane from a mini-batch of samples. The anchors of the c -th lane, A_c can be selected according to,

$$A_c = \{(i, j) | GT_{(i,j)} = c, s_\theta(x^{in})_{(i,j,c)} \geq \mu_c, i \in [0, H], j \in [0, W]\}, \quad (7)$$

$$V_c = \{V_{(i,j)} | (i, j) \in A_c\}, \quad (8)$$

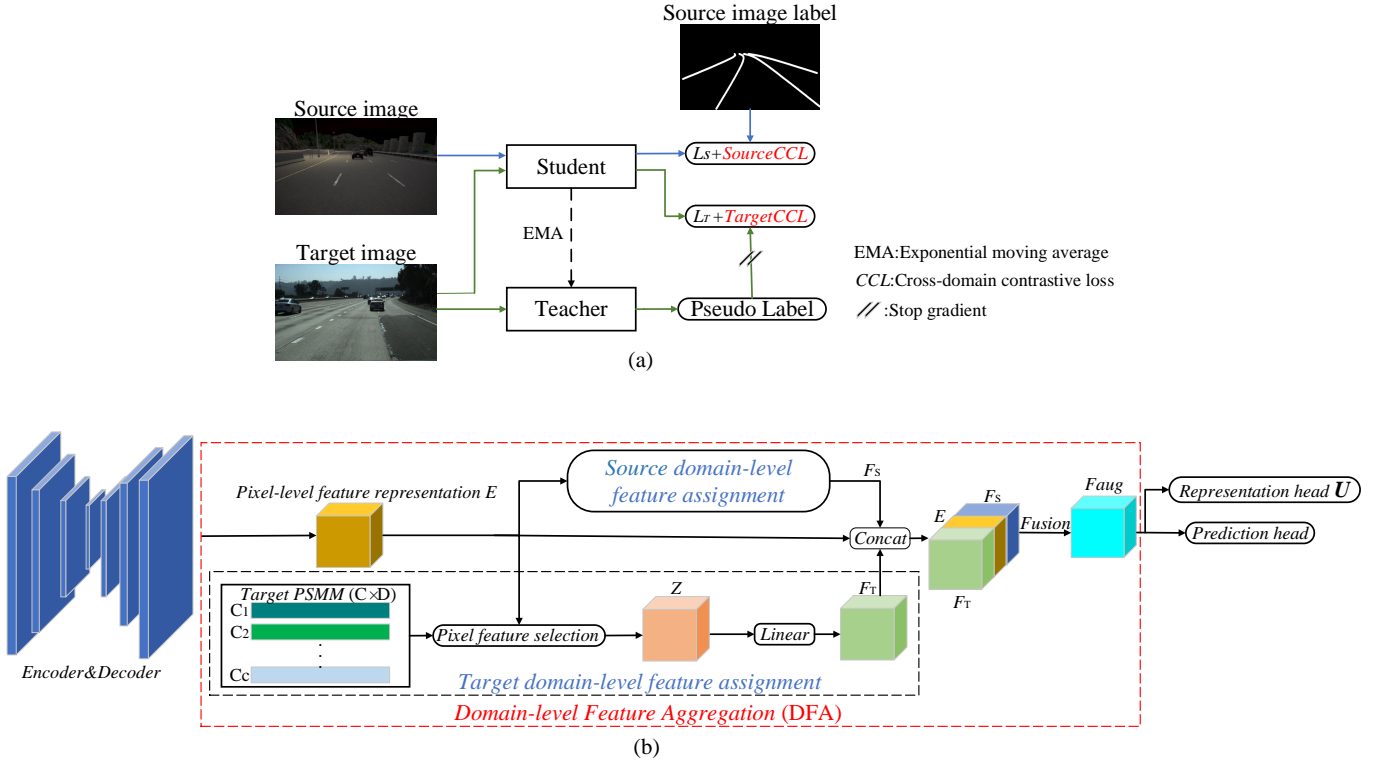


Fig. 2: An overview of DACCA’s framework. (a) Training pipeline of DACCA. (b) Student/Teacher model structure. The source domain-level feature assignment shares the same structure with the target domain-level feature assignment, except that a PSMM saves features from the source domain. The representation head U is used to obtain the pixel-wise feature representation.

where GT denotes the labels in the source domain or pseudo-labels in the target domain, x^{in} represents an input image, and μ_c is the threshold. We set pixels whose GT are category c and whose predicted confidence are greater than μ_c as anchors to reduce the effect of hard anchors. $V \in R^{H \times W \times D}$ is the pixel-wise representation and D is the feature dimension. As illustrated in Fig. 2 (b), we achieve V by exploiting an extra representation head U . U shares the input with the prediction head and is only used in the training process. V_c is the set of feature representation of anchors and $V_{cp} \in R^D$ is randomly selected from V_c .

Positive Sample Selection. To ensure the appropriate assignment of positive samples, we establish a positive sample memory module (PSMM) for each lane in both the source and target domains to save its domain-level feature, denoted as $B_{so} \in R^{C \times D}$ and $B_{ta} \in R^{C \times D}$. We initialize and update the domain-level features saved in PSMM, following MCIBI [32]. For the c -th lane, we take its domain-level feature as the feature representation of the positive sample.

$$V_c^+ = B_o(c), \quad (9)$$

where o is the source domain (so) or the target domain (ta).

Feature Initialization. The process of initializing and updating features is the same for source and target PSMM. We take the target PSMM as an example to describe this process. MCIBI [32] selects the feature representation of one pixel for each lane to initialize the feature in PSMM. However, this way may bring out false feature initialization due to false pseudo

labels. For the c -th lane, we initialize its feature in PSMM using the center of the features of all anchors, expressed by,

$$B_{ta}(c) = \frac{1}{|V_c|} \sum_{n_c \in V_c} n_c, \quad (10)$$

where $|V_c|$ denotes the number of anchors and n_c is the feature representation of anchors in V_c .

Feature Update. The features in target PSMM are updated through the EMA after each training iteration m ,

$$(B_{ta}(c))_m = t_{m-1} \times (B_{ta}(c))_{m-1} + (1 - t_{m-1}) \times \partial((V_c)_{m-1}), \quad (11)$$

where t is the scale factor and ∂ is used to transform V_c to obtain the feature with the same size as $(B_{ta}(c))_{m-1}$. Following MCIBI, we adopt the polynomial annealing policy to schedule t ,

$$t_m = (1 - \frac{m}{T})^p \times (t_0 - \frac{t_0}{100}) + \frac{t_0}{100}, m \in [0, T], \quad (12)$$

where T is the total number of training iterations. We set both p and t_0 as 0.9 empirically. To implement ∂ , we first compute the cosine similarity vector S_c between the feature representation of anchors in $(V_c)_{m-1}$ and $(B_{ta}(c))_{m-1}$, as below,

$$S_c(i) = \frac{(V_c)_{m-1}(i) \times (B_{ta}(c))_{m-1}}{\|(V_c)_{m-1}(i)\|_2 \times \|(B_{ta}(c))_{m-1}\|_2}, i \in [1, |V_c|], \quad (13)$$

where we use (i) to index the element in S_c or feature representation in $(V_c)_{m-1}$. Then, we obtain the output of $\partial((V_c)_{m-1})$ by,

$$\partial((V_c)_{m-1}) = \sum_{i=1}^{|V_c|} \frac{1 - S_c(i)}{\sum_{j=1}^{|V_c|} (1 - S_c(j))} \times (V_c)_{m-1}(i). \quad (14)$$

For the source PSMM, features in V_c come from the source domain.

Negative Sample Selection. We directly use pixels of a lane not labeled c as the negative samples in the source domain. On the other hand, in the target domain, pixels with the lowest predicted confidence for category c are selected as negative samples.

$$\text{neg_loc}_c = \{(i, j) \mid \operatorname{argmin}_{c' \in c^*} (s_\theta(x_T^k)_{(i,j,c')}) = c, \quad (15)$$

$$i \in [0, W], j \in [0, H]\},$$

$$\text{neg}_c = \{V_{(i,j)} \mid (i, j) \in \text{neg_loc}_c\}, \quad (16)$$

where neg_loc_c and neg_c denote the location and the set of feature representation of negative samples of class c , respectively. $V_{cpq}^- \in R^D$ is also randomly selected from neg_c . To compare intra-domain and inter-domain features at the same time, we propose a Cross-domain Contrastive Loss (CCL), consisting of an intra-domain contrastive learning loss L_{inter} and an inter-domain contrastive learning loss L_{intra} .

$$CCL = L_{inter} + L_{intra}, \quad (17)$$

where L_{inter} and L_{intra} are the same as Eq. 6. CCL is applied in both source and target domains. For the source cross-domain contrastive loss (SCCL), the positive samples in L_{inter} are the domain-level features saved in B_{ta} , and the positive samples in L_{intra} are the domain-level features saved in B_{so} . The positive samples in the target cross-domain contrastive loss (TCCL) are opposite to SCCL. The overall loss of DACCA is,

$$\text{Loss} = \frac{1}{N_s} \sum_{k=1}^{N_s} (\lambda_c \times SCCL^k + L_S^k) + \frac{1}{N_t} \sum_{k=1}^{N_t} (\lambda_c \times TCCL^k + L_T^k), \quad (18)$$

where λ_c is the scale factor, which is set to 0.1 empirically.

C. Domain-level Feature Aggregation

Cross-domain context dependency is essential to transfer knowledge across domains. Cross-domain Contextual Feature Aggregation (CCFA) is an effective way to achieve cross-domain context dependency. Existing CCFA methods [11], [34], [33] only aggregate a mini-batch of features. We argue that aggregating features from a whole domain is more beneficial. As shown in Fig. 2 (b), Domain-level Feature Aggregation (DFA) aims to fuse the domain-level features into the pixel-level representation. DFA contains two key components, i.e., source and target domain-level feature assignment. The process is the same for both. We take the target domain-level feature assignment as an example to depict the process.

Pixel Feature Selection. To select the corresponding domain-level feature for each lane pixel, we propose the pixel



Fig. 3: Location of unreliable background pixels in green.

feature selection. We first obtain the predicted category at location (i, j) by,

$$P = \operatorname{argmax}_{c' \in c^*} (\operatorname{Softmax}(\operatorname{Conv}(E))_{(i,j,c')}), i \in [0, W], j \in [0, H], \quad (19)$$

where $E \in R^{H \times W \times D}$ represents the feature map, containing the pixel-level feature representation. 1×1 convolution (termed as Conv) is adopted to change the channels of E to $C + 1$. $P \in R^{H \times W}$ saves the predicted category at each location of E . Then, we build a feature map Z whose pixel values are zero and whose size and dimension are the same as E . We assign the pixel-wise feature to Z using the domain-level feature.

$$Z_{(i,j)} = B_{ta}(P_{(i,j)}), P_{(i,j)} \neq C + 1, i \in [0, W], j \in [0, H]. \quad (20)$$

After the assignment, Z is a domain-level feature map. Here, the lane pixels on E predicted as the background in training are called unreliable background pixels (UBP). For example, as illustrated in Fig. 3, UBP is mainly located at the edge of the lane. However, the features of UBP can not be augmented since domain-level features are only aggregated for the foreground pixels. To refine the features of UBP, we also perform further feature aggregation on UBP.

Specifically, the predicted confidence of the UBP is usually low, hence we distinguish UBP from reliable background pixels by setting confidence threshold ε . The UBP is defined as,

$$UBP = \{(i, j) \mid \text{pred}_{(i,j)} < \varepsilon, P_{(i,j)} = C + 1, i \in [0, W], j \in [0, H]\}, \quad (21)$$

where $\text{pred}_{(i,j)}$ is the confidence of the predicted category at location (i, j) . $\text{pred}_{(i,j)}$ is obtained by: $\text{pred}_{(i,j)} = \max_{c' \in c^*} (\operatorname{Softmax}(\operatorname{Conv}(E))_{(i,j,c')})$. We choose the category with the lowest Euclidean distance as the pseudo category of UBP and use domain-level feature of pseudo category to instantiate UBP in Z .

$$P_{(i,j)} = \operatorname{argmin}_{c' \in c^*} \left(\text{dis} \left(E_{(i,j)}^{UBP}, B_{ta}(c') \right) \right), (i, j) \in UBP, \quad (22)$$

$$Z_{(i,j)} = B_{ta}(P_{(i,j)}), (i, j) \in UBP, \quad (23)$$

where $E_{(i,j)}^{UBP}$ is the feature representation of UBP at location (i, j) in E , and dis is used to calculate the Euclidean distance between the feature representation of UBP and the domain-level feature.

Thereafter, we adopt a linear layer to extract features along the channel dimension in Z to obtain the output of target

domain-level feature assignment F_T . In the same process, we replace the target PSMM with the source PSMM to obtain the feature F_S . F_S , F_T , and E are concatenated along the channel dimension and fused by a 1×1 convolution to enrich the cross-domain context information of E .

$$F_{aug} = \text{Conv}(\varphi(E, F_S, F_T)), \quad (24)$$

where $F_{aug} \in R^{H \times W \times D}$ is the aggregated features and φ is the concatenate operation.

IV. EXPERIMENTS

A. Experimental Setting

Datasets. We conduct extensive experiments to examine DACCA on six datasets for lane detection tasks, i.e., TuLane [35], MoLane [35], MuLane [35], CULane [1], Tusimple [36], and OpenLane [37]. The source domain of the TuLane dataset uses 24,000 labeled simulated images as the training set, and the target domain images derives from the Tusimple dataset. The source domain of the MoLane dataset uses 80,000 labeled simulated images as the training set, and the target domain training set is adopted from the real scenes and contains 43,843 unlabeled images. The MuLane dataset mixes the TuLane and MoLane datasets are uniformly blended. The source domain of MuLane dataset uses 48000 labeled simulated images as the training set, and the target domain combines the Tusimple and MoLane target domains.

Following [7], we conduct the experiments on "CULane to Tusimple" and "Tusimple to CULane". "Tusimple to CULane" means that the source domain is Tusimple and the target domain is CULane. To further validate the effectiveness of our method on the domain adaptation cross difficult scenes, we carry out the experiments on "CULane to OpenLane" and "OpenLane to CULane". CULane dataset [1] is a large scale lane detection dataset, consisting of 88880, 9675, and 34680 frames for training set, validation set, and testing set. Tusimple [36] dataset is small scale dataset for lane detection. It has 3626 training images and 2782 testing images. OpenLane [37] is a comprehensive benchmark for 2D and 3D lane detection, which is composed of 200K frames with 14 kinds of categories, complex lane structures, and five kinds of weather.

Evaluation Metrics. For TuLane, MuLane, MoLane, and Tusimple datasets. We use three official indicators to evaluate the model performance for three datasets: Accuracy, false positives (FP), and false negatives (FN). Accuracy is defined by $Accuracy = \frac{p_c}{p_y}$, where p_c denotes the number of correct predicted lane points and p_y is the number of ground truth lane points. A lane point is regarded as correct if its distance is smaller than the given threshold $t_{pc} = \frac{20}{\cos(a_{yl})}$, where a_{yl} represents the angle of the corresponding ground truth lane. We measure the rate of false positives with $FP = \frac{l_f}{l_p}$ and the rate of false positives with $FN = \frac{l_m}{l_y}$, where l_f is the number of mispredicted lanes, l_p is the number of predicted lanes, l_m is the number of missing lanes and l_y is the number of ground truth lanes. Following [35], we consider lanes as mispredicted if the Accuracy $< 85\%$. For CULane and OpenLane, we adopt the F1 score to measure the performance,

TABLE I: Results of critical components.

Source-only	SCCL	Self-Training	TCCL	DFA	UBP	Accuracy(%)	FP(%)	FN(%)
✓						77.42	58.29	54.19
✓	✓					79.63	53.41	50.00
✓	✓	✓				80.76	49.39	47.50
✓	✓	✓	✓			81.77	48.36	45.06
✓	✓	✓	✓	✓		82.43	44.53	42.89
✓	✓	✓	✓	✓	✓	83.99	42.27	40.10

$F_1 = \frac{2 \times Precision \times Recall}{Precision + Recall}$, where $Precision = \frac{TP}{TP + FP}$ and $Recall = \frac{TP}{TP + FN}$, where TP denote the true positives.

Implementation Details. We update the learning rate by the Poly policy with power factor $1 - (\frac{iter}{total_iter})^{0.9}$. We select the AdamW optimizer with the initial learning rate 0.0001. We adopt the data augmentation of random rotation and flip for TuLane, and random horizontal flips and random affine transforms (translation, rotation, and scaling) for MuLane and MoLane. The training epochs on the TuLane, MuLane, MoLane, "CULane to Tusimple", "Tusimple to CULane", "CULane to OpenLane", and "OpenLane to CULane" are 30, 20, 20, 20, 12, 50, and 50 respectively. We set the threshold for filtering false pseudo labels α_c to 0.3 during domain adaptation. The threshold for selecting anchors μ_c and UBP ε are 0.2 and 0.7, respectively. The number of anchors M and negative samples N in the cross-domain contrastive loss are 256 and 50, respectively. Temperature hyper-parameter τ is set to 0.07 empirically. The feature dimension D is 128. The optimizer and update policy of the learning rate are the same as those in pretraining. All images are resized to 384×800 . All experiments are conducted on a single Tesla V100 GPU with 32 GB memory. DACCA is implemented based on PPLanedet [38].

B. Ablation Study

We ablate the key components of DACCA and use SCNN with ResNet50 [39] as the detection model. If not specified, all ablation studies are conducted on TuLane.

Effectiveness of cross-domain contrastive learning (CCL). In Table I, when only source domain data are used in supervised learning, SCCL prompts the accuracy from 77.42% to 79.63%. It also indicates that our SCCL works for supervised training. On the other hand, the accuracy increases by 1.01%, i.e., from 80.76% to 81.77%, if TCCL is adopted. T-SNE visualization in Fig. 7 (c) shows that the model with CCL can learn more discriminative features.

Effectiveness of domain-level feature aggregation (DFA). In Table I, DFA can improve the detection accuracy from 81.77% to 82.43%. As for feature aggregation of UBP, the accuracy is further increased by 1.56% (83.99% vs. 82.43%). Also, we can observe a significant adaptation of the source and target domain features in Fig. 5 (c), which validates the effectiveness of domain-level feature aggregation.

Generalizability of different methods. As shown in Table II, our method can be integrated into various segmentation-based lane detection methods. In SCNN, using our method can increase the accuracy by 6.57% and decrease FP and FN by 16.02% and 14.09%, respectively. Also, in the lightweight model ERFNet, the accuracy rises by 7.17%, and FP and

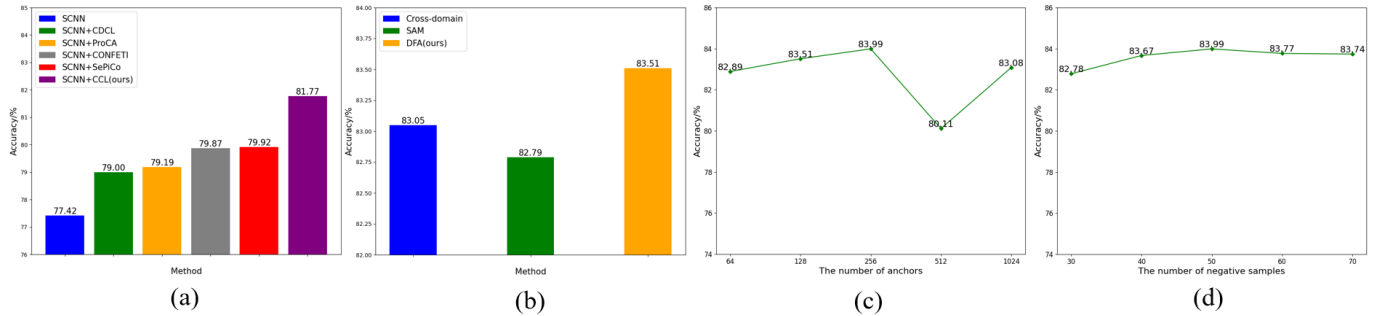


Fig. 4: (a) Comparison among existing contrastive loss variants. (b) Comparison among existing cross-domain context aggregation. (c) Study of the number of anchors. (d) Study of the number of negative samples.

TABLE II: Generalizability of different methods. The symbol * indicates source domain only.

Model	Backbone	Accuracy/%	FP/%	FN/%
SCNN*	ResNet50	77.42	58.29	54.19
SCNN+DACCA	ResNet50	83.99	42.27	40.10
ERFNet [40]*	ERFNet	83.30	37.46	37.55
ERFNet+DACCA	ERFNet	90.47	30.66	18.16
RTFormer [41]*	RTFormer-Base	87.24	26.78	25.17
RTFormer+DACCA	RTFormer-Base	92.24	15.10	12.58

FN drop by 6.8% and 19.39%. Finally, in the Transformer-based method RTFormer, our method significantly improves the detection performance, in terms of accuracy, FP, and FN.

Comparison with existing contrastive loss variants. In Fig. 4 (a), CCL is evaluated against other contrastive loss variants in UDA. In turn, we replace CCL in DACCA with CDCL, ProCA [25], CONFETI [23], and SePiCo [42]. Compared with ProCA and CONFETI, CCL increases the accuracy by 2.58% (81.77% vs. 79.19%) and 1.9% (81.77% vs. 79.87%), respectively. The reason may be that both ProCA and CONFETI ignore the differences in feature distribution between the source domain and target domain and only use a prototype to represent the features of the two domains. Moreover, CCL overwhelms SePiCo regarding accuracy. It attributes to SePiCo only taking domain-level features from the source domain as the positive samples but ignoring the samples from the target domain.

Comparison with existing cross-domain context aggregation. We substitute the DFA with Cross-domain [11] and Self-attention module (SAM) [33]—the latter aggregate features in a mini-batch. The superiority of the DFA is shown in Fig. 4 (b). DFA performs better than Cross-domain and SAM, e.g., prompts the accuracy by 0.46% (83.51% vs. 83.05%) and 0.72% (83.51% vs. 82.79%), respectively. From the T-SNE visualization in Fig. 6, we can see that DFA aligns the features of two domains better. The results demonstrate that aggregating features from the whole domain is more effective than from a mini-batch.

The number of anchors M . We study the influence of the number of anchors M and the results are shown in Fig. 4 (c). It can be observed that the model achieves the best performance when M is 256. Besides, It causes extra computational burden when M increases. Considering

TABLE III: The threshold for selecting anchors.

μ_c	Accuracy/%	FP/%	FN/%
0.0	80.97	51.72	46.95
0.1	81.27	51.45	46.84
0.2	83.99	42.27	40.10
0.3	80.79	50.81	46.52
0.4	80.80	52.14	49.25

TABLE IV: The threshold for selecting UBP.

ε	Accuracy/%	FP/%	FN/%
-	83.32	46.83	40.76
0.5	83.41	44.79	40.67
0.6	83.38	46.67	40.17
0.7	83.99	42.27	40.10
0.8	82.20	47.55	43.53
0.9	81.66	48.49	45.34

accuracy and computational burden, we set M as 256.

The number of negative samples N . Fig. 4 (d) shows the influence of the number of negative samples. When N is 50, model achieves the best performance. We can also see that as N increases, the accuracy does not always improve, indicating that excessive negative samples can degrade performance.

The threshold for selecting anchors μ_c . We study the threshold for selecting anchors μ_c . As shown in Table III, setting the anchor selection threshold can avoid hard anchors compared with anchor selection without the threshold (83.99% vs. 80.97%). However, when the threshold is too high, available anchors shrink, leading to performance degradation (83.99% vs. 80.80%). Hence, we set μ_c to 0.2.

The threshold for selecting UBP. We can see that without the feature refinement of UBP, accuracy is only 83.32% in Table IV. When ε is 0.7, model achieves the best performance. It has little effect on model performance when ε is too low. This is attributed to the small number of UBP. When ε is too high, many background pixels are wrongly regarded as UBP, causing the negative effect.

The threshold for filtering false pseudo labels. We study the threshold for filtering false pseudo labels α_c and results are shown in Table V. When α_c is low, false pseudo labels have a greater impact on performance. If α_c is too high, the

TABLE V: The threshold for filtering false pseudo labels.

α_c	Accuracy/%	FP/%	FN/%
0.1	81.39	52.36	48.02
0.2	82.37	48.25	45.81
0.3	83.99	42.27	40.10
0.4	83.58	44.41	42.10
0.5	83.49	45.09	42.79

TABLE VI: The way of feature aggregation.

Way	Accuracy/%	FP/%	FN/%
Add	77.92	52.72	54.04
Weighted add	80.05	49.15	48.23
Concatenation	83.99	42.27	40.10

number of pseudo labels is too small, providing insufficient supervision signals. Therefore, we set α_c to 0.3.

The way of feature fusion. We study the way of feature fusion in Table VI. Add denotes for element-wise adding E , F_S , and F_T . Compared with add, concatenation gains 6.07% accuracy improvements. The reason may be that Add directly changes the original pixel features but concatenation does not. Weighted add means adding E , F_S , and F_T weightedly where weights are predicted by a 1×1 convolution. Concatenation overwhelms Weighted add regarding accuracy, FN, and FP. We adopt the concatenation as the way of feature fusion.

C. Visualization of cross-domain features

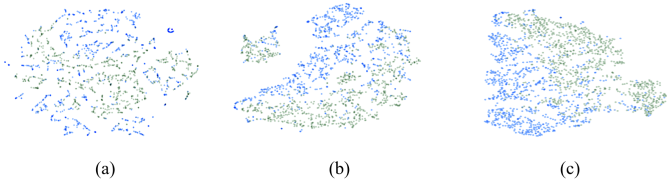


Fig. 5: T-SNE visualization of the key components. (a) SCNN trained with only source domain. (b) SCNN trained with SCCL and TCCL. (c) SCNN trained with SCCL, TCCL, and DFA. Blue and green color represent the source and target domain, respectively.



Fig. 6: T-SNE visualization of different cross-domain context aggregation methods. (a) Cross-domain. (b) SAM. (c) DACCA.

T-SNE visualization of the key components. As shown in Fig. 5 (a). There is a slight adaptation of cross-domain features when model is only trained in the source domain. Learned cross-domain features are aligned better using our

proposed CCL in Fig. 5 (b). However, since CCL is a pixel-wise contrast, it can lead to the separation of the feature space due to lack of contextual information. To solve this problem, we enhance the links between cross-domain features by introducing domain-level feature aggregation (DFA). DFA incorporate cross-domain contextual information into the pixel-wise feature and effectively address the separation of the feature space in Fig. 5 (c).

T-SNE visualization of different cross-domain context aggregation methods. Compared with Cross-domain [11] and Self-attention module (SAM) [33], DACCA aligns source and target domain features better in Fig. 6, indicating domain-level features can provide more cross-domain knowledge than features from a mini-batch.

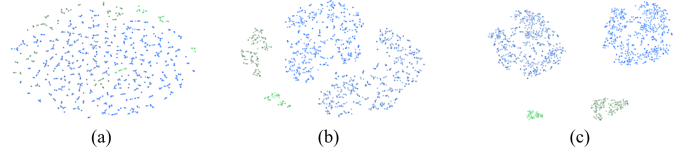


Fig. 7: T-SNE visualization of different loss functions. (a) Cross-entropy loss. (b) SePiCo [42]. (c) CCL. Different colors represent different lane features.

T-SNE visualization of different loss functions. As shown in Fig. 7, our CCL learns more discriminative features than SePiCo [42], indicating that our sample selection policy is effective. Besides, cross-entropy is inefficient in discriminating features of different categories. Our CCL can effectively compensate for the deficiency of cross-entropy loss.

D. Comparison with state-of-the-art methods

Performance on TuLane. The results on TuLane are shown in Table X. When ERFNet is used as the detection model, our method performs better than other methods. For instance, our method outperforms MLDA in terms of accuracy by 2.04% (90.47% vs. 88.43%). Besides, using our CCL and DFA, the performance of MLDA gains consistent improvement. It indicates our sample selection policy is more effective than designing complicated loss functions, and DFA has a stronger domain adaptive ability than AIEM in MLDA. Regarding FN metrics, our method is 5.97% and 4.11% lower than PyCDA and Cross-domain, respectively. Significantly, when using the Transformer model RTFormer, DACCA outperforms the state-of-the-art SGPCS (92.24% vs. 91.55%) and achieves the best experimental results on TuLane in similar settings.

Performance on OpenLane to CULane. To further validate our method’s generalization ability, we carry out experiments transferring from OpenLane to CULane to demonstrate a domain adaptation between difficult real scenarios. As shown in Table IX, our method delivers 4.2% enhancement (43.0% vs. 38.8%) compared to the state-of-the-art MLDA. Our DACCA surpasses the existing methods in most indicators and also all these results reflect its outperformance.

Performance on CULane to Tusimple. As presented in Table XI, our DACCA achieves the best performance on “CULane to Tusimple”. For instance, DACCA increases the

TABLE VII: Performance comparison on "CULane" to "OpenLane". Detection model and backbone are still ERFNet.

Method	All	Up&Down	Curve	Extreme Weather	Night	Intersection	Merge&Split
Advent [7]	17.3	12.6	15.8	20.7	16.9	9.4	15.6
PyCDA [43]	17.0	12.8	15.4	19.2	16.0	9.6	14.9
Maximum Squares [44]	18.9	13.4	16.0	21.4	17.3	11.0	16.8
MLDA [7]	22.3	18.4	20.3	24.8	21.4	15.8	21.0
DACCA	27.6	25.0	25.3	31.8	27.0	14.1	23.9

TABLE VIII: Performance comparison on "Tusimple" to "CULane". Detection model and backbone are still ERFNet. We only report the number of false positives for Cross category following [7].

Method	Normal	Crowded	Night	No line	Shadow	Arrow	Dazzle	Curve	Cross	Total
Advent [7]	49.3	24.7	20.5	18.4	16.4	34.4	26.1	34.9	6257	30.4
PyCDA [43]	41.8	19.9	13.6	15.1	13.7	27.8	18.2	29.6	4422	25.1
Maximum Squares [44]	50.5	27.2	20.8	19.0	20.4	40.1	27.4	38.8	10324	31.0
MLDA [7]	61.4	36.3	27.4	21.3	23.4	49.1	30.3	43.4	11386	38.4
DACCA	64.6	39.1	28.6	24.5	25.8	52.0	33.4	42.9	8517	41.9

TABLE IX: Performance comparison on "OpenLane" to "CULane".

Method	Normal	Crowded	Night	No line	Shadow	Arrow	Dazzle	Curve	Cross	Total
Advent [7]	51.2	24.5	21.5	19.9	16.9	34.7	27.2	35.3	5789	31.7
PyCDA [43]	42.4	20.6	14.7	15.9	14.4	28.6	19.5	30.8	4452	26.3
Maximum Squares [44]	51.4	28.4	22.1	19.7	20.9	40.8	28.1	39.3	9813	31.8
MLDA [7]	62.0	38.0	28.5	21.9	24.1	50.3	31.7	44.5	11399	38.8
DACCA	64.9	39.6	29.3	25.1	26.3	52.8	34.1	43.5	7158	43.0

TABLE X: Performance comparison on TuLane.

Method	Detection model	Backbone	Accuracy/%	FP/%	FN/%
DANN [13]	ERFNet	ERFNet	86.69	33.78	23.64
ADDA [13]	ERFNet	ERFNet	87.90	32.68	22.33
SGADA [13]	ERFNet	ERFNet	89.09	31.49	21.36
SGPCS [13]	ERFNet	ERFNet	89.28	31.47	21.48
SGPCS	RTFormer	RTFormer-Base	90.78	28.44	15.66
SGPCS	UFLD	ResNet18	91.55	28.52	16.16
LD-BN-ADAPT [45]	UFLD	ResNet18	92.00	-	-
MLDA [7]	ERFNet	ERFNet	88.43	31.69	21.33
MLDA+CCL	ERFNet	ERFNet	89.00	30.53	20.42
MLDA+DFA	ERFNet	ERFNet	89.45	30.22	20.02
PyCDA [43]	ERFNet	ERFNet	86.73	31.26	24.13
Cross-domain [11]	ERFNet	ERFNet	88.21	29.17	22.27
Maximum Squares [44]	ERFNet	ERFNet	85.98	30.20	26.85
DACCA	ERFNet	ERFNet	90.47	30.66	18.16
DACCA	RTFormer	RTFormer-Base	92.24	15.10	12.58

TABLE XI: Performance comparison on "CULane" to "Tusimple".

Method	Detection model	Backbone	Accuracy/%	FP/%	FN/%
Advent [7]	ERFNet	ERFNet	77.1	39.7	43.9
PyCDA [43]	ERFNet	ERFNet	80.9	51.9	45.1
Maximum Squares [44]	ERFNet	ERFNet	76.0	38.2	42.8
MLDA [7]	ERFNet	ERFNet	89.7	29.5	18.4
DACCA	ERFNet	ERFNet	92.1	26.7	14.6

accuracy from 89.7% to 92.1% compared with the state-of-the-art method MLDA. It indicates our DACCA can perform well on the domain adaptation from difficult scene to simple scene.

Performance on MoLane. Next, our method is tested on MoLane. By observing Table XII, we can conclude that DACCA is superior to existing unsupervised domain-adaptive lane detection methods. Specifically, DACCA improves the accuracy by 2.22% against SGPCS (93.50% vs. 91.28%).

TABLE XII: Performance comparison on MoLane. Symbol * indicates source domain only.

Method	Detection model	Backbone	Accuracy/%	FP/%	FN/%
DANN [13]	ERFNet	ERFNet	85.65	22.25	22.25
ADDA [13]	ERFNet	ERFNet	87.85	18.61	18.66
SGADA [13]	ERFNet	ERFNet	89.46	15.13	15.13
SGPCS [13]	ERFNet	ERFNet	90.08	12.16	12.16
SGPCS [13]	RTFormer	RTFormer-Base	91.28	8.69	8.69
LD-BN-ADAPT [45]	UFLD	ResNet18	92.68	-	-
MLDA [7]	ERFNet	ERFNet	89.97	12.33	15.42
PyCDA [43]	ERFNet	ERFNet	87.40	17.59	18.10
Cross-domain [11]	ERFNet	ERFNet	88.57	15.16	17.41
Maximum Squares [44]	ERFNet	ERFNet	87.22	21.31	27.85
DACCA*	ERFNet	ERFNet	86.15	23.85	29.50
DACCA	ERFNet	ERFNet	90.52	7.00	13.95
DACCA*	RTFormer	RTFormer-Base	86.77	20.6	26.9
DACCA	RTFormer	RTFormer-Base	93.50	6.26	7.25

TABLE XIII: Performance comparison on MuLane. Symbol * indicates source domain only.

Method	Detection model	Backbone	Accuracy/%	FP/%	FN/%
DANN [13]	ERFNet	ERFNet	84.01	38.31	36.30
ADDA [13]	ERFNet	ERFNet	85.99	29.38	28.59
SGADA [13]	ERFNet	ERFNet	85.26	29.13	28.73
SGPCS [13]	ERFNet	ERFNet	86.92	27.49	28.39
SGPCS [13]	RTFormer	RTFormer-Base	88.02	23.98	25.80
LD-BN-ADAPT [45]	UFLD	ResNet18	89.88	-	-
MLDA [7]	ERFNet	ERFNet	87.28	32.59	30.06
PyCDA [43]	ERFNet	ERFNet	86.01	35.15	34.17
Cross-domain [11]	ERFNet	ERFNet	85.74	32.10	37.42
Maximum Squares [44]	ERFNet	ERFNet	84.26	42.59	49.67
DACCA*	ERFNet	ERFNet	83.28	47.17	55.21
DACCA	ERFNet	ERFNet	87.93	25.95	27.08
DACCA*	RTFormer	RTFormer-Base	84.19	37.88	39.20
DACCA	RTFormer	RTFormer-Base	90.14	15.11	17.14

Moreover, using ERFNet as the detection model, DACCA improves the accuracy by 4.37% (90.52% vs. 86.15%) compared to the model using only source domain data. It is worth

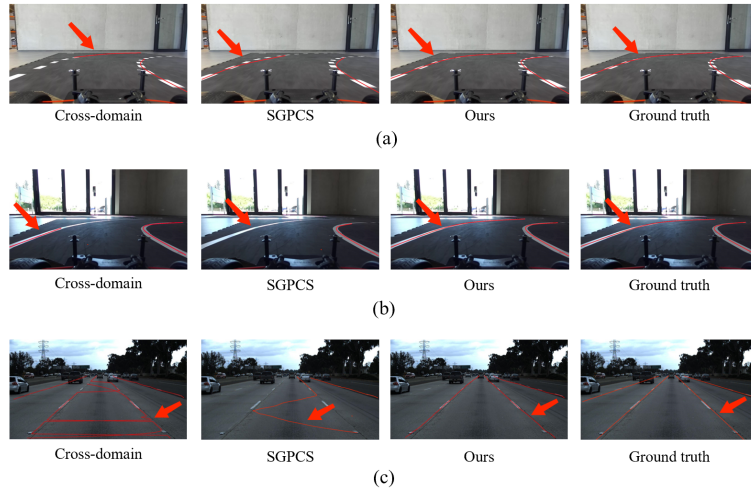


Fig. 8: Visualization result comparison among cross-domain, SGPCS, and our method. Results on (a) MuLane, (b) MoLane, and (c) TuLane.

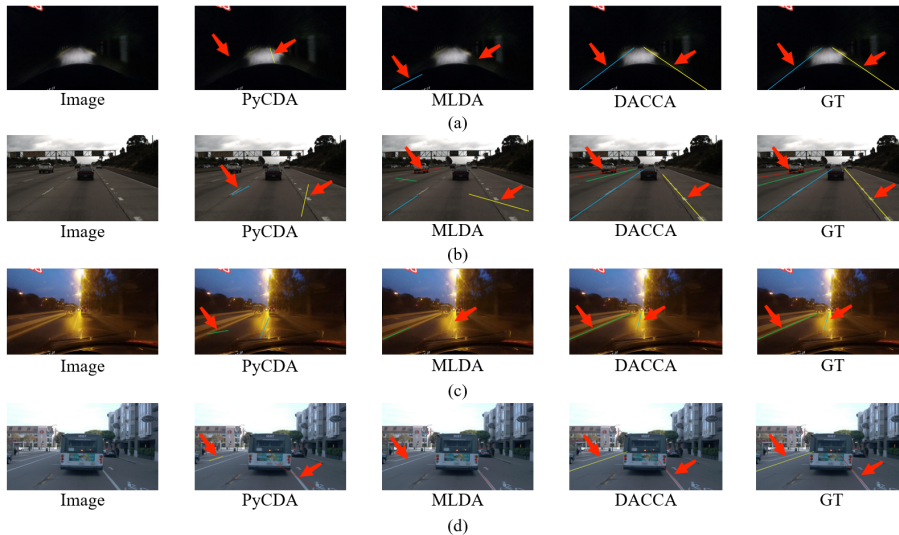


Fig. 9: Visualization result comparison among PyCDA, MLDA, and our DACCA. Results on (a) Tusimple to CULane, (b) CULane to Tusimple, (c) OpenLane to CULane, and (d) CULane to OpenLane.

mentioning that if the Transformer model, RTFormer, is used as the detection model, the detection accuracy can be prompted by 6.73% (93.50% vs. 86.77%).

Performance on MuLane. To further validate our method’s generalization ability, we carry out experiments on MuLane. As shown in Table XIII, when using ERFNet as the detection model, our method delivers 4.65% enhancement (87.93% vs. 83.28%) in contrast to the model using only the source domain data. Moreover, our method DACCA outperforms existing methods in accuracy, FP, and FN. Specifically, DACCA is 1.92% higher than PyCDA in accuracy (87.93% vs. 86.01%), 6.15% lower than Cross-domain in FP (25.95% vs. 32.10%), and 7.09% lower than PyCDA in FN (27.08% vs. 34.17%). All these results reflect the outperformance of our method.

Performance ob Tusimple to CULane. We conduct the experiments on the domain adaptation from simple scene and difficult scene and result are shown in Table VIII. DACCA demonstrates consistent performance advantages.

Performance on CULane to OpenLane. From Table VII, we can see that DACCA achieves the best performance and gains 5.3% F1 score improvement. The results on domain adaptation cross difficult scenes manifest the effectiveness and generalizability of our DACCA.

Qualitative evaluation. The visualization comparison results are illustrated in Figs. 8 and 9. In Fig. 8 (c) and Fig. 9 (b), our method predicts more smooth lanes than the other methods in urban scenarios. Our method can detect the complete lanes in real-world scenes, as shown in Fig. 8 and Fig. 9 (a), (c), and (d). Qualitative results demonstrate that our method can effectively transfer knowledge across domains.

V. CONCLUSION

This paper presents a novel unsupervised domain-adaptive lane detection via contextual contrast and aggregation (DACCA), in which learning discriminative features and

transferring knowledge across domains are exploited. Firstly, we create the positive sample memory module to preserve the domain-level features of the lane. Then, we propose a cross-domain contrastive loss to improve feature discrimination of different lanes by a novel sample selection strategy without modifying the form of contrastive loss. Finally, we propose the domain-level feature aggregation to fuse the domain-level features with the pixel-level features to enhance cross-domain context dependency. Experimental results show that our approach achieves the best performance, compared with existing methods, on TuLane, or transferring from CULane to Tusimple, Tusimple to CULane, CULane to OpenLane, and OpenLane to CULane. Moreover, on MuLane and MoLane datasets, our method outperforms existing unsupervised domain-adaptive segmentation-based lane detection methods.

Furthermore, although DACCA is established upon the segmentation-based lane detection, it holds considerable potential for application in other lane detection methods, e.g., keypoint-based and transformer-based ones. Our future work is to explore this aspect.

REFERENCES

- [1] X. Pan, J. Shi, P. Luo, X. Wang, and X. Tang, "Spatial as deep: Spatial cnn for traffic scene understanding," in *Proceedings of the AAAI Conference on Artificial Intelligence*, 2018, pp. 7276–7283.
- [2] H. Xu, S. Wang, X. Cai, W. Zhang, X. Liang, and Z. Li, "Curvelane-nas: Unifying lane-sensitive architecture search and adaptive point blending," in *European Conference on Computer Vision*, 2020, pp. 689–704.
- [3] G. Liu, F. Wörgöter, and I. Markelić, "Combining statistical hough transform and particle filter for robust lane detection and tracking," in *2010 IEEE Intelligent Vehicles Symposium*, 2010, pp. 993–997.
- [4] K. Saito, K. Watanabe, Y. Ushiku, and T. Harada, "Maximum classifier discrepancy for unsupervised domain adaptation," in *Proceedings of the IEEE/CVF Conference on Computer Vision and Pattern Recognition*, 2018, pp. 3723–3732.
- [5] T.-H. Vu, H. Jain, M. Bucher, M. Cord, and P. Pérez, "Advent: Adversarial entropy minimization for domain adaptation in semantic segmentation," in *Proceedings of the IEEE/CVF Conference on Computer Vision and Pattern Recognition*, 2019, pp. 2517–2526.
- [6] A. Tarvainen and H. Valpola, "Mean teachers are better role models: Weight-averaged consistency targets improve semi-supervised deep learning results," *Advances in Neural Information Processing Systems*, vol. 30, 2017.
- [7] C. Li, B. Zhang, J. Shi, and G. Cheng, "Multi-level domain adaptation for lane detection," in *Proceedings of the IEEE/CVF Conference on Computer Vision and Pattern Recognition*, 2022, pp. 4380–4389.
- [8] M. Vayyat, J. Kasi, A. Bhattacharya, S. Ahmed, and R. Tallamraju, "Cluda: Contrastive learning in unsupervised domain adaptation for semantic segmentation," *arXiv preprint arXiv:2208.14227*, 2022.
- [9] K. He, H. Fan, Y. Wu, S. Xie, and R. Girshick, "Momentum contrast for unsupervised visual representation learning," in *Proceedings of the IEEE/CVF Conference on Computer Vision and Pattern Recognition*, 2020, pp. 9729–9738.
- [10] T. Chen, S. Kornblith, M. Norouzi, and G. Hinton, "A simple framework for contrastive learning of visual representations," in *International Conference on Machine Learning*, 2020, pp. 1597–1607.
- [11] J. Yang, W. An, C. Yan, P. Zhao, and J. Huang, "Context-aware domain adaptation in semantic segmentation," in *Proceedings of the IEEE/CVF Winter Conference on Applications of Computer Vision*, 2021, pp. 514–524.
- [12] N. Garnett, R. Uziel, N. Efrat, and D. Levi, "Synthetic-to-real domain adaptation for lane detection," in *Proceedings of the Asian Conference on Computer Vision*, 2020.
- [13] J. Gebele, B. Stuhr, and J. Haselberger, "Carlane: A lane detection benchmark for unsupervised domain adaptation from simulation to multiple real-world domains," *arXiv preprint arXiv:2206.08083*, 2022.
- [14] T. Zheng, H. Fang, Y. Zhang, W. Tang, Z. Yang, H. Liu, and D. Cai, "Resa: Recurrent feature-shift aggregator for lane detection," in *Proceedings of the AAAI Conference on Artificial Intelligence*, 2021, pp. 3547–3554.
- [15] L. T. Torres, R. F. Berriel, T. M. Paixão, C. Badue, A. F. De Souza, and T. Oliveira-Santos, "Keep your eyes on the lane: Attention-guided lane detection," *arXiv preprint arXiv:2010.12035*, 2020.
- [16] L. Liu, X. Chen, S. Zhu, and P. Tan, "Condlanenet: a top-to-down lane detection framework based on conditional convolution," in *Proceedings of the IEEE/CVF International Conference on Computer Vision*, 2021, pp. 3773–3782.
- [17] L. Tabelini, R. Berriel, T. M. Paixao, C. Badue, A. F. De Souza, and T. Oliveira-Santos, "Polylanenet: Lane estimation via deep polynomial regression," in *2020 25th International Conference on Pattern Recognition (ICPR)*. IEEE, 2021, pp. 6150–6156.
- [18] R. Liu, Z. Yuan, T. Liu, and Z. Xiong, "End-to-end lane shape prediction with transformers," in *Proceedings of the IEEE/CVF winter conference on applications of computer vision*, 2021, pp. 3694–3702.
- [19] Z. Qin, H. Wang, and X. Li, "Ultra fast structure-aware deep lane detection," in *European Conference on Computer Vision*, 2020, pp. 276–291.
- [20] R. Gong, W. Li, Y. Chen, and L. V. Gool, "Dlow: Domain flow for adaptation and generalization," in *Proceedings of the IEEE/CVF Conference on Computer Vision and Pattern Recognition*, 2019, pp. 2477–2486.
- [21] M. Sajjadi, M. Javanmardi, and T. Tasdizen, "Regularization with stochastic transformations and perturbations for deep semi-supervised learning," *Advances in Neural Information Processing Systems*, pp. 1163–1171, 2016.
- [22] R. Wang, Z. Wu, Z. Weng, J. Chen, G.-J. Qi, and Y.-G. Jiang, "Cross-domain contrastive learning for unsupervised domain adaptation," *IEEE Transactions on Multimedia*, vol. 112, no. 9, pp. 3473–3496, 2023.
- [23] T. Li, S. Roy, H. Zhou, H. Lu, and S. Lathuilière, "Contrast, stylize and adapt: Unsupervised contrastive learning framework for domain adaptive semantic segmentation," in *Proceedings of the IEEE/CVF Conference on Computer Vision and Pattern Recognition*, 2023, pp. 4868–4878.
- [24] W. Wang, T. Zhou, F. Yu, J. Dai, E. Konukoglu, and L. Van Gool, "Exploring cross-image pixel contrast for semantic segmentation," in *Proceedings of the IEEE/CVF International Conference on Computer Vision*, 2021, pp. 7303–7313.
- [25] Z. Jiang, Y. Li, C. Yang, P. Gao, Y. Wang, Y. Tai, and C. Wang, "Prototypical contrast adaptation for domain adaptive semantic segmentation," in *European Conference on Computer Vision*, 2022, pp. 36–54.
- [26] F. Zhang, V. Koltun, P. Torr, R. Ranfil, and S. R. Richter, "Unsupervised contrastive domain adaptation for semantic segmentation," *arXiv preprint arXiv:2204.08399*, 2022.
- [27] L. Melas-Kyriazi and A. K. Manrai, "Pixmatch: Unsupervised domain adaptation via pixelwise consistency training," in *Proceedings of the IEEE/CVF Conference on Computer Vision and Pattern Recognition*, 2021, pp. 12 435–12 445.
- [28] C. Hu, S. Hudson, M. Ethier, M. Al-Sharman, D. Rayside, and W. Melek, "Sim-to-real domain adaptation for lane detection and classification in autonomous driving," in *2022 IEEE Intelligent Vehicles Symposium (IV)*. IEEE, 2022, pp. 457–463.
- [29] L.-C. Chen, G. Papandreou, I. Kokkinos, K. Murphy, and A. L. Yuille, "DeepLab: Semantic image segmentation with deep convolutional nets, atrous convolution, and fully connected crfs," *IEEE Transactions on Pattern Analysis and Machine Intelligence*, vol. 40, no. 4, pp. 834–848, 2017.
- [30] H. Zhao, J. Shi, X. Qi, X. Wang, and J. Jia, "Pyramid scene parsing network," in *Proceedings of the IEEE/CVF Conference on Computer Vision and Pattern Recognition*, 2017, pp. 2881–2890.
- [31] Y. Yuan, X. Chen, and J. Wang, "Object-contextual representations for semantic segmentation," in *European Conference on Computer Vision*, 2020, pp. 173–190.
- [32] Z. Jin, T. Gong, D. Yu, Q. Chu, J. Wang, C. Wang, and J. Shao, "Mining contextual information beyond image for semantic segmentation," in *Proceedings of the IEEE/CVF International Conference on Computer Vision*, 2021, pp. 7231–7241.
- [33] I. Chung, J. Yoo, and N. Kwak, "Exploiting inter-pixel correlations in unsupervised domain adaptation for semantic segmentation," in *Proceedings of the IEEE/CVF Winter Conference on Applications of Computer Vision*, 2023, pp. 12–21.
- [34] Q. Zhou, Z. Feng, Q. Gu, J. Pang, G. Cheng, X. Lu, J. Shi, and L. Ma, "Context-aware mixup for domain adaptive semantic segmentation," *IEEE Transactions on Circuits and Systems for Video Technology*, vol. 33, no. 2, pp. 804–817, 2022.

- [35] B. Stuhr, J. Haselberger, and J. Gebele, "Carlane: A lane detection benchmark for unsupervised domain adaptation from simulation to multiple real-world domains," *Advances in Neural Information Processing Systems*, pp. 4046–4058, 2022.
- [36] "Tusimple dataset," <https://github.com/TuSimple/tusimple-benchmark>, accessed on 11th August 2023.
- [37] L. Chen, C. Sima, Y. Li, Z. Zheng, J. Xu, X. Geng, H. Li, C. He, J. Shi, Y. Qiao *et al.*, "Persformer: 3d lane detection via perspective transformer and the openlane benchmark," in *European Conference on Computer Vision*. Springer, 2022, pp. 550–567.
- [38] K. Zhou, "Pplanedet, a toolkit for lane detection based on paddlepaddle," <https://github.com/zkyseu/PPlanedet>, 2022.
- [39] K. He, X. Zhang, S. Ren, and J. Sun, "Deep residual learning for image recognition," in *Proceedings of the IEEE/CVF Conference on Computer Vision and Pattern Recognition*, 2016, pp. 770–778.
- [40] E. Romera, J. M. Alvarez, L. M. Bergasa, and R. Arroyo, "Erfnet: Efficient residual factorized convnet for real-time semantic segmentation," *IEEE Transactions on Intelligent Transportation Systems*, vol. 19, no. 1, pp. 263–272, 2017.
- [41] J. Wang, C. Gou, Q. Wu, H. Feng, J. Han, E. Ding, and J. Wang, "Rtformer: Efficient design for real-time semantic segmentation with transformer," pp. 7423–7436, 2022.
- [42] B. Xie, S. Li, M. Li, C. H. Liu, G. Huang, and G. Wang, "Sepico: Semantic-guided pixel contrast for domain adaptive semantic segmentation," *IEEE Transactions on Pattern Analysis and Machine Intelligence*, vol. 45, no. 7, pp. 9004–9021, 2023.
- [43] Q. Lian, F. Lv, L. Duan, and B. Gong, "Constructing self-motivated pyramid curriculums for cross-domain semantic segmentation: A non-adversarial approach," in *Proceedings of the IEEE/CVF International Conference on Computer Vision*, 2019, pp. 6758–6767.
- [44] M. Chen, H. Xue, and D. Cai, "Domain adaptation for semantic segmentation with maximum squares loss," in *Proceedings of the IEEE/CVF International Conference on Computer Vision*, 2019, pp. 2090–2099.
- [45] K. Bhardwaj, Z. Wan, A. Raychowdhury, and R. Goldhahn, "Real-time fully unsupervised domain adaptation for lane detection in autonomous driving," in *2023 Design, Automation & Test in Europe Conference & Exhibition (DATE)*, 2023, pp. 1–2.



Jun Li (Senior Member, IEEE) received his Ph.D. degree in control theory and control engineering from Southeast University (SEU), Nanjing, China, in 2007.

From 2008 to 2010, he was a Post-Doctoral Fellow at SEU. In 2014, he was a Visiting Scholar with the New Jersey Institute of Technology, Newark, NJ, USA. He is the Director of the Robotics and Intelligent Systems Laboratory at School of Automation, SEU. His current research interests include machine vision, logistics and construction robotics, machine

learning, and operations research.

Professor Li is a Fellow of the Institution of Engineering and Technology (IET) and serves as an Associate Editor for IEEE TRANSACTIONS ON INTELLIGENT TRANSPORTATION SYSTEMS.



Kunyang Zhou received his B.S. degree in electrical engineering and automation from Nantong University, Nantong, China, in 2022. He is currently pursuing his M.S. degree in Control Science and Engineering from Southeast University. His current research interests include deep learning and pattern recognition.



Yunjian Feng received his M.S. degree in vehicle electronics engineering from Wuhan University of Technology, Wuhan, China, in 2020. He is currently pursuing his Ph.D. degree in control theory and control engineering from Southeast University. His current research interests include machine vision, deep learning, and autonomous driving.